3D Printing of Polytetrafluoroethylene Hollow Needles for Medical Applications

Roger Sachan¹, Andrew Sachan¹, Junqi Lu³, Detlev Erdmann⁴, Jennifer Y. Zhang^{3,5}, Roger J. Naravan⁶

¹ Department of Chemistry, North Carolina State University, Raleigh, NC, USA

² Wake Technical Community College, Raleigh, NC, USA

³ Department of Dermatology, Duke University Medical Center, Durham, North Carolina, USA

⁴ Division of Plastic, Maxillofacial and Oral Surgery, Duke University Medical Center, Durham, North Carolina, USA

⁵ Department of Dermatology, Duke University Medical Center, Durham, North Carolina, USA

⁶ Department of Biomedical Engineering, University of North Carolina and North Carolina State University, Raleigh, NC, USA

Contact Author:

Roger J Narayan, MD, PhD

Professor

UNC/NCSU Joint Department of Biomedical Engineering

Box 7115

Raleigh, NC 27695-7115

T: 1 919 696 8488

F: 1 509 696 8481

E: roger narayan@ncsu.edu

Abstract:

The delivery of drugs or vaccines using hollow needles involves a "poke and flow" approach,

which involves the movement of the drug or vaccine through the bore of a hollow needle. In this

paper, hollow needle arrays were created out of the fluoropolymer polytetrafluoroethylene using

a digital light processing (DLP)-based 3D printing process. Confocal laser scanning microscopy

revealed that the hollow needles in the three-by-one hollow needle array contained sharp tips,

uniform heights, and hollow bores. X-ray photoelectron spectroscopy and Raman spectroscopy

revealed that the elemental composition and carbon bonding of the 3D printed

polytetrafluoroethylene matched that of bulk polytetrafluoroethylene, respectively. The reduced

elastic modulus of the needle material, 1.94+/-0.22 GPa, is appropriate for skin penetration and is

similar to that previously described for bulk polytetrafluoroethylene. The needle array was used

to deliver methyl blue, a model drug, to surgically-discarded human abdomen skin. These results

suggest that DLP-based 3D printing of polytetrafluoroethylene may be an appropriate approach

for producing needle arrays and other technologically-relevant devices.

Keywords: polytetrafluoroethylene, digital light processing, 3D printing, drug delivery

2

Introduction:

Polytetrafluoroethylene is a synthetic fluoropolymer of tetrafluoroethylene that is prepared from tetrafluoroethylene by a free-radical polymerization approach [1]. The unusual properties of polytetrafluoroethylene are attributed to the chemical properties of fluorine, which include a small van der Waals radius (1.32 Å)), large electronegativity, low polarizability, and the ability to form strong (485 kJ·mol⁻¹) bonds with carbon [1, 2].

Polytetrafluoroethylene is considered to be an ideal material for medical devices such as drug delivery devices since it exhibits many desirable properties for tissue-medical device interactions. For example, neither water nor water-based materials is capable of wetting polytetrafluoroethylene; this feature minimizes undesirable adsorption and retention of the drug on the surface of a drug delivery device [3]. In addition, polytetrafluoroethylene exhibits one of the lowest coefficients of friction values of any solid material (0.08–0.10); its inherent lubricity and nonstick behavior obviate the need for surface modification (e.g., the application of a silicone coating) to enhance lubricity and reduce friction [4, 5]. Other medically-relevant properties of polytetrafluoroethylene include exceptional heat resistance (e.g., a continuous-use temperature below 260 °C), excellent barrier properties that extend the shelf life of products, and exceptional electrical properties (e.g., a low dielectric constant and high insulation resistance) [6, 7, 8]. Polytetrafluoroethylene also exhibits a high degree of bioinertness, resistance to microbiological and enzymatic degradation, and exceptional chemical resistance (e.g., little or no formation of leachables and extractables) among thermoplastic polymers [9, 10]. It shows reactivity with only a few chemicals, including gaseous fluorine, molten alkali metals, metal hydrides, and organic halogenated compounds (e.g., chlorine trifluoride and oxygen difluoride). Polytetrafluoroethylene has found use in many types of medical devices, including artificial

blood vessels, catheters (e.g., catheters for the delivery of nickel-titanium alloy treatment rods), material for plastic surgery implants, membranes for use in the oral cavity, scaffolds (e.g., structures for the repair of ligaments and tendons), stents, and surgical meshes [11-15].

It is difficult to process polytetrafluoroethylene because its rigid chain structure is associated with a high melt viscosity and a high melting temperature (~320 °C); these properties preclude extrusion-based 3D printing and injection molding [16, 17]. Polytetrafluoroethylene is commonly processed via a powder processing approach in which a cold compacted-powder is sintered [18]. Several recent efforts have been made to process polytetrafluoroethylene and polytetrafluoroethylene composites using 3D printing methods. In 2016, O'Keefe and Luscombe used aerosol deposition to process polytetrafluoroethylene-polyacrylate composite films containing polytetrafluoroethylene-polyacrylate core-shell nanoparticles for microwave device applications; they showed that the dielectric constant of the film decreased as the polytetrafluoroethylene content in the film increased [19]. More recently, Jiang et al. used a direct ink writing method to process an ink that contained an aqueous dispersion of surfactantstabilized polytetrafluoroethylene nanoparticles and a binding gum; a thermal treatment process was used to remove the gum and surfactant to create the final polytetrafluoroethylene part [20]. Zhang et al. used digital ultraviolet lithography to process a solution that contained a dispersion of polytetrafluoroethylene nanoparticles in a photocurable solution of polyethylene glycol diacrylate; sintering was used to remove the polyethylene glycol diacrylate and obtain the final polytetrafluoroethylene part [21, 22]. Droplet whispering gallery mode microcavities and electrostatic drivable biomimetic devices were prepared using this approach [22]. Other studies have also examined the use of vat polymerization to create polytetrafluoroethylene-containing parts. For example, Slatnick et al. used a digital light processing-based vat polymerization

approach to process aliphatic urethane acrylate oligomers that contained polytetrafluoroethylene and two other solid lubricants, graphite and molybdenum disulfide [23]. The inclusion of polytetrafluoroethylene in the composite was associated with low coefficient of friction and wear rate values.

In this study, we consider a digital light processing-based vat polymerization approach with an approximately 50 µm voxel size to create polytetrafluoroethylene parts for medical device applications, specifically a hollow needle array for transdermal drug delivery [24]. Confocal laser scanning microscopy, X-ray photoelectron spectroscopy, Raman spectroscopy, nanoindentation, and a skin penetration study with discarded human abdomen skin were used to understand the properties of a 3D printed three-by-one hollow needle array. The results of this study show the promise of three-by-one hollow needle arrays that were made using digital light processing-based vat polymerization for drug or vaccine delivery.

Experimental Procedure:

Three-by-one hollow needle arrays and the base on which they sat were made from polytetrafluoroethylene using digital light processing-based vat polymerization from a polytetrafluoroethylene solution (3M, Minneapolis, Minnesota). Digital light processing-based vat polymerization involves the use of a digital micromirror device, which contains an array of several microscale mirrors with the capability of being rotated in an independent manner, to define the specific pattern for illumination and selective polymerization of the polytetrafluoroethylene solution [25]. It is important to note that the final polymerized polytetrafluoroethylene is an input ingredient in the printing formulation; polytetrafluoroethylene

does not undergo additional polymerization during the 3D printing process. The printing formulation, including photopolymerizable binder(s), is proprietary. The photopolymerizable binders were polymerized during the 3D printing process; they were removed after the 3D printing process via thermal processing.

The needle morphology, including needle height, was assessed using a VKx1100 confocal laser scanning microscope (Keyence, Osaka, Japan). Measurements of the needle array were taken by standing the array on its base and taking a top-down 3D profilometry measurement, and by lying the needle array on its side and taking a planar optical image. A SPECS X-ray photoelectron spectroscopy with PHOIBOS 150 Hemispherical Analyzer (SPECS Surface Nano Analysis GmbH, Berlin, Germany) was used to obtain elemental composition data from the base of the needle arrays. Raman spectroscopy measurements were used to understand carbon bonding in the base of the needle arrays; the Raman data was obtained using an XploRA plus confocal Raman microscope (Horiba Ltd., Kyoto, Japan) with laser excitation at a 532 nm wavelength and a 1024 pixel×256 pixel Horiba Scientific CCD detector. Reduced modulus and hardness values were obtained from the base of the needle array using a Bruker Hysitron TI980 Triboindenter (Billerica, MA); a diamond conospherical (conical) tip with a 1 µm radius of curvature was used for data acquisition. The sample was tested under the displacement control approach with a maximum depth of 1 µm, a load time of 20 s, a hold time at the maximum depth of 30 s, and an unload time of 20 s. To understand the tissue penetration properties of the needle array, surgically discarded human abdomen skin was collected in compliance with a Duke University institutional review board (IRB) procedure [26]. The skin was minimally processed other than being removed from the body and carefully cut away from the bulk of fat tissues. The subcutaneous fat tissues were scraped off using surgical tweezers and scissors; the skin was then washed with phosphate-buffered saline (PBS) and wiped dry using a Kimwipe. The needle array was preloaded with methyl blue using a 0.5 ml insulin syringe. The skin was laid in a petri dish with the epidermal side facing up; the skin was then perforated by the needle array and wiped dry with a Kimwipe to remove excess dye. Bright field images were obtained using a BX41 microscopic imaging system (Olympus, Center Valley, PA).

Results and Discussion:

Confocal laser scanning microscopy has previously been used to understand the topographical features of drug delivery devices [27]. Confocal laser scanning micrographs of the three-by-one polytetrafluoroethylene needle array are shown in Figure 1((a)-(d)). Figure 1 (a) shows an optical micrograph of the needle array in a planar orientation, Figure 1 (b) shows a topdown view of the bore of a single needle with a line that indicates the path of the profilometry scan, Figure 1 (c) shows a profile of the needle height along the scan, and Figure 1 (d) shows a 3d representation of the top-down view of the bore of a single needle. The hollow passage in the hollow needles, which is intended for drug delivery from the device through the skin surface, was a net shape that was obtained by the 3D printing process. The average needle height in the needle array as determined from an image of the needle array in the planar orientation was noted to be 4.59 mm +/- 0.03 mm; the average needle height in the needle array as determined from profilometry of the three needles in the needle array in the top-down orientation was noted to be 4.66 mm+/-0.01 mm. The difference in needle height values as determined from the two measurement approaches may be attributed to the roughness of the needle array substrate; the roughness is attributed to the \sim 50 μ m voxel size that is associated with the 3D printing approach. The needles showed sharp needle tips and good needle-to-needle uniformity. A bulge in one of

the needles was associated with a scratch from the instrument that was used to transfer the sample to the microscope for imaging. The needle bores were noted to be hollow from imaging of the needles in the top-down orientation.

X-ray photoelectron spectroscopy data collected from the base of the needle array revealed the presence of carbon, fluorine, and a small amount of oxygen (Figure 2). The C:O atomic ratio of 0.5 is consistent with the composition of the –CF₂– monomer and is similar to that previously described by Girardeux and Pireaux for polytetrafluoroethylene [28]. The presentation of oxygen in the spectrum is attributed to the adsorption of oxygen on the needle array surface; according to Vandencasteele et al., oxygen contamination can reach 8% in polytetrafluoroethylene [29]. No other impurities were noted, including those of concern for skin contact applications. The Raman spectrum from the base of the needle array is shown in Figure 3. The peaks at 289.56 cm⁻¹ and 383.81 cm⁻¹ are associated with the twisting and bending modes of CF₂ in polytetrafluoroethylene, respectively; the peak at 732.73 cm⁻¹ is associated with the symmetric stretching mode of CF₂ in polytetrafluoroethylene [30]. The peaks at 1218.1 cm⁻¹, 1300.23 cm⁻¹, and 1382.44 cm⁻¹ are attributed to C-C rock, C-C wag, and C-C symmetrical stretch modes, respectively [31].

The mean and standard deviation values were calculated from thirty data points. Nanoindentation of the base of the needle array revealed that the material exhibited a reduced Young's modulus value of 1.94 +/- 0.22 GPa and a hardness value 77.87 +/- 6.53 MPa. These values are similar to those previously described by Tang et al. and Wyszkowska et al. for bulk polytetrafluoroethylene [32, 33]. It should be noted that Park et al. indicated that microneedles that were manufactured from materials with Young's moduli exceeding ~1 GPa generally exhibit fracture forces that exceed skin penetration forces [34].

To examine the skin penetration properties of the needle array for topical drug or vaccine delivery, we used surgically discarded human skin samples and methyl blue dye as previously described [26]. Figure 4 (a) and (b) contain light microscopy images, which demonstrate the delivery of methyl blue in human abdomen skin treated by the needle array. An image taken at 4 × magnification is shown in Figure 4(a), and an image taken at 10 × magnification is shown in Figure 4(b). The brightfield images of the needle array-treated skin showed effective penetration of the skin by the needle array. This result showed that the needle array was effective for human skin penetration, which enabled the delivery of the model drug.

Conclusions:

Three-by-one hollow needle arrays were made from polytetrafluoroethylene by a digital light processing-based 3D printing process. Confocal laser scanning microscopy showed that the needles exhibited sharp tips, good needle-to-needle uniformity, and hollow bores. X-ray photoelectron spectroscopy revealed the presence of fluorine, carbon, and oxygen as well as the absence of toxic impurities in the 3D printed polytetrafluoroethylene; the amounts of carbon and oxygen in the needle material matched those expected for polytetrafluoroethylene. Raman spectroscopy data from the 3D printed polytetrafluoroethylene indicated the presence of carbon-carbon and carbon-fluorine bonding that was consistent with the bonding seen in polytetrafluoroethylene. The reduced elastic modulus of the needle material was noted to be appropriate for use in skin penetration devices. The needle array successfully delivered the model drug methyl blue to human abdomen skin. These results suggest that the digital light processing-based 3D printing process provides a viable and scalable pathway for manufacturing

microscale transdermal drug delivery devices, including needle arrays for the delivery of drugs and vaccines, and other types of medical devices.

Conflict of interest statement:

On behalf of all authors, the corresponding author states that there is no conflict of interest.

Data availability:

The datasets generated during and/or analyzed during the current study are available from the corresponding author on reasonable request.

References

- 1. G.J. Puts, P. Crouse and B.M. Ameduri, *Chem. Rev.*, 119, 1763-1805 (2019).
- 2. T.A. Blanchet, *Polymer Tribology*, 347-374 (2009).
- 3. M. Feng, K. Ghafoor, B. Seo, K. Yang and J. Park, *Innov. Food Sci. Emerg. Technol.*, 19, 133-139 (2013).
- 4. J. Liu, J. Yang, W. Wang, S. Fu, Y. Shi and H. Men, Sens. Mater., 28, 785-795 (2016).
- 5. M. Abdul Samad, *Polymers.*, 13, 608 (2021).
- 6. H. Yasuoka, M. Yoshida, K. Sugita, K. Ohdaira, H. Murata and H. Matsumura, *Thin Solid Films*, 516, 687-690 (2008).
- 7. B.D. Matthews, B.L. Pratt, H.S. Pollinger, C.L. Backus, K.W. Kercher, R.F. Sing and B.T. Heniford, *J. Surg. Res.*, 114, 126-132 (2003).
- 8. V.F. Cardoso, D.M. Correia, C. Ribeiro, M.M. Fernandes and S. Lanceros-Méndez, *Polymers*, 10, 161 (2018).
- 9. L. Tong, D.T. Kwok, H. Wang, L. Wu and P.K. Chu, *Adv. Eng. Mater.*, 12, B163-B169 (2010).
- 10. S. Ebnesajjad, Introduction to fluoropolymers. In Applied Plastics Engineering Handbook (pp. 55-71). William Andrew Publishing (2017).
- 11. H.A. Marouf and H.M. El-Guindi, *Oral Surg. Oral Med. Oral Pathol. Oral Radiol. Endod.*, 89, 164-170 (2000).
- 12. S. Sack, P. Kahlert and R. Erbel, Minim. Invasive Ther. Allied Technol., 18, 156-163 (2009).
- 13. M.M. Sattar, M. Patel and A. Alani, *Br. Dent. J.*, 222, 151-158 (2017).
- 14. J.M. Carbonell, I.S. Martín, A. Santos, A. Pujol, J.D. Sanz-Moliner and J. Nart, *Int. J. Oral Maxillofac. Surg.*, 43, 75-84 (2014).
- 15. A.J. Rigby, S.C. Anand and A.R. Horrocks, *J. Textile Inst.*, 88, 83-93 (1997).
- 16. T. Shyr, W. Chung, W. Lu and A. Lin, Europ. Polym. J., 72, 50-63 (2015).
- 17. H. Teng, Appl. Sci., 2, 496-512 (2012).
- 18. S.S. Hambir, J.P. Jog and V.M. Nadkarni, Polym. Eng. Sci., 34, 1065-1069 (1994).
- 19. S. O'Keefe and C.K. Luscombe, *Polym. Int.*, 65, 820-826 (2016).
- 20. Z. Jiang, O. Erol, D. Chatterjee, W. Xu, N. Hibino, L.H. Romer, S.H. Kang and D.H. Gracias, *ACS Appl. Mater. Interfaces*, 11, 28289-28295 (2019).

- 21. Y. Zhang, M. Yin, O. Xia, A.P. Zhang and H. Tam, Optical 3D μ-printing of polytetrafluoroethylene (PTFE) microstructures. In 2018 IEEE Micro Electro Mechanical Systems (MEMS) (pp. 37-40). IEEE.
- 22. Y. Zhang, M. Yin, X. Ouyang, A.P. Zhang and H. Tam, *Appl. Mater. Today*, 19, 100580 (2020).
- 23. J. Slapnik, T. Stiller, T. Wilhelm and A. Hausberger, *Lubricants*, 8, 104 (2020).
- 24. Scott, C. (2016). 3M Develops New Patent-Pending Technology for the 3D Printing of Fluoropolymers. https://3dprint.com/149969/3m-3d-printing-fluoropolymers/. Published September 21, 2016.
- 25. S.A. Skoog, P.L. Goering and R.J. Narayan, *J. Mater. Sci. Mater. Med.*, 25, 845-856 (2014).
- 26. A. Sachan, R.J. Sachan, J. Lu, H. Sun, Y.J. Jin, D. Erdmann, J.Y. Zhang and R.J. Narayan, MRS Advances, 6, 61-65 (2021).
- 27. R. Sachan, P. Jaipan, J.Y. Zhang, S. Degan, D. Erdmann, J. Tedesco, L. Vanderwal, S.J. Stafslien, I. Negut and A. Visan, *Int. J. Bioprinting*, 3 (2017).
- 28. C. Girardeaux and J. Pireaux, Surf. Sci. Spectra, 4, 138-141 (1996).
- 29. N. Vandencasteele, D. Merche and F. Reniers, Surf. Interface Anal., 38, 526-530 (2006).
- 30. V. Rastogi, U. Rao, S. Chaurasia, A.K. Mishra, H.K. Poswal, M.N. Deo and S.M. Sharma, 1731, 060025 (2016).
- 31. D. Vavlekas, L. Melo, M. Ansari, E. Grant, F. Fremy, J.L. McCoy and S.G. Hatzikiriakos, *Polym. Test.*, 61, 65-73 (2017).
- 32. E. Wyszkowska, M. Leśniak, L. Kurpaska, R. Prokopowicz, I. Jozwik, M. Sitarz and J. Jagielski, *J. Mol. Struct.*, 1157, 306-311 (2018).
- 33. G. Tang, X. Ma, M. Sun and X. Li, *Carbon*, 43, 345-350 (2005).
- 34. J. Park, M.G. Allen and M.R. Prausnitz, J. Controlled Release, 104, 51-66 (2005).

Figure Captions

Figure 1. Confocal laser scanning micrographs of the three-by-one polytetrafluoroethylene needle array. (a) An optical micrograph of the needle array in a planar orientation. (b) A top-down optical image of the bore of a single needle with a line that indicates the path of the profilometry scan. (c) A profile of the needle height along the scan. (d) A 3D representation of the top-down view of the bore of a single needle.

Figure 2. X-ray photoelectron spectrum from the base of the needle array.

Figure 3. Raman spectrum from the base of the needle array.

Figure 4. Light microscopy images from the delivery of methyl blue in human skin that was treated by the needle array. (a) Image taken at $4 \times$ magnification. (b) Image taken at $10 \times$ magnification.

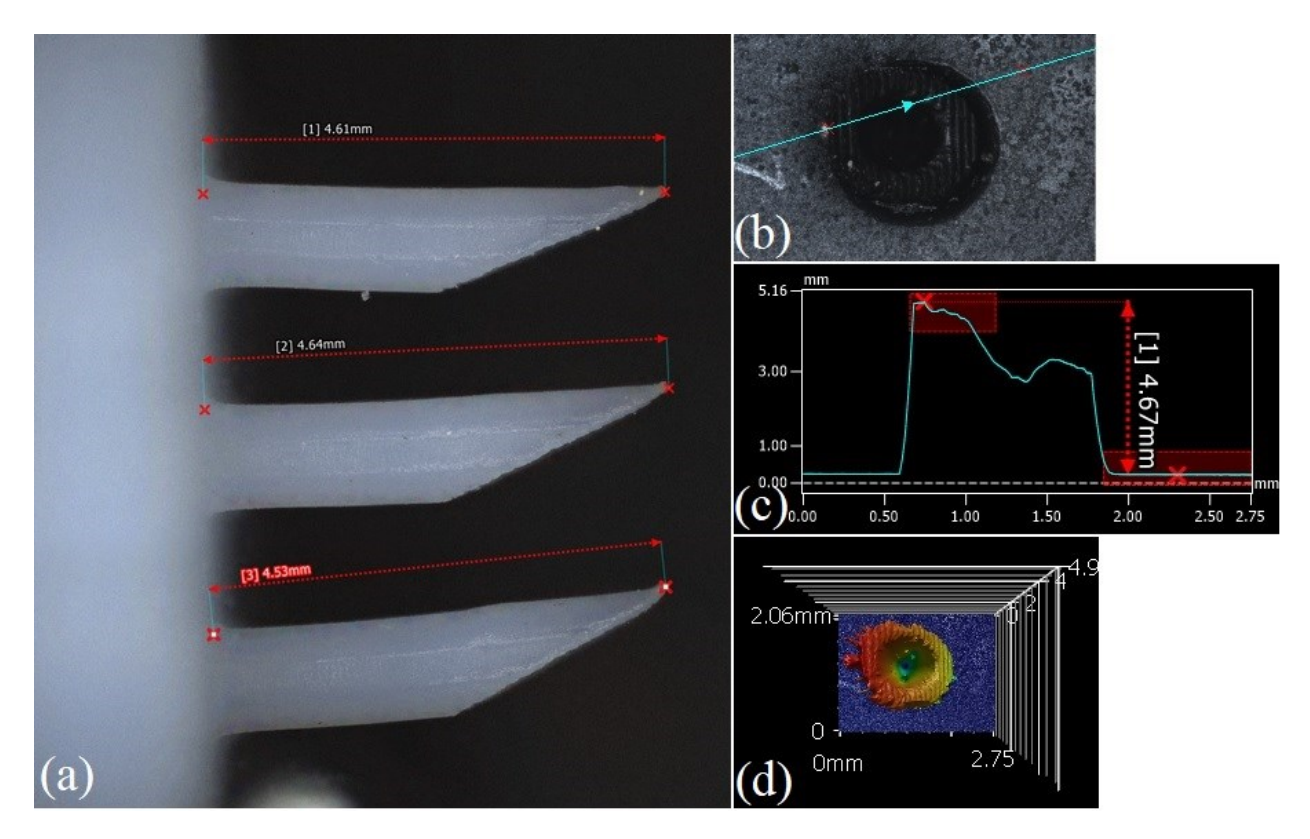


Figure 1

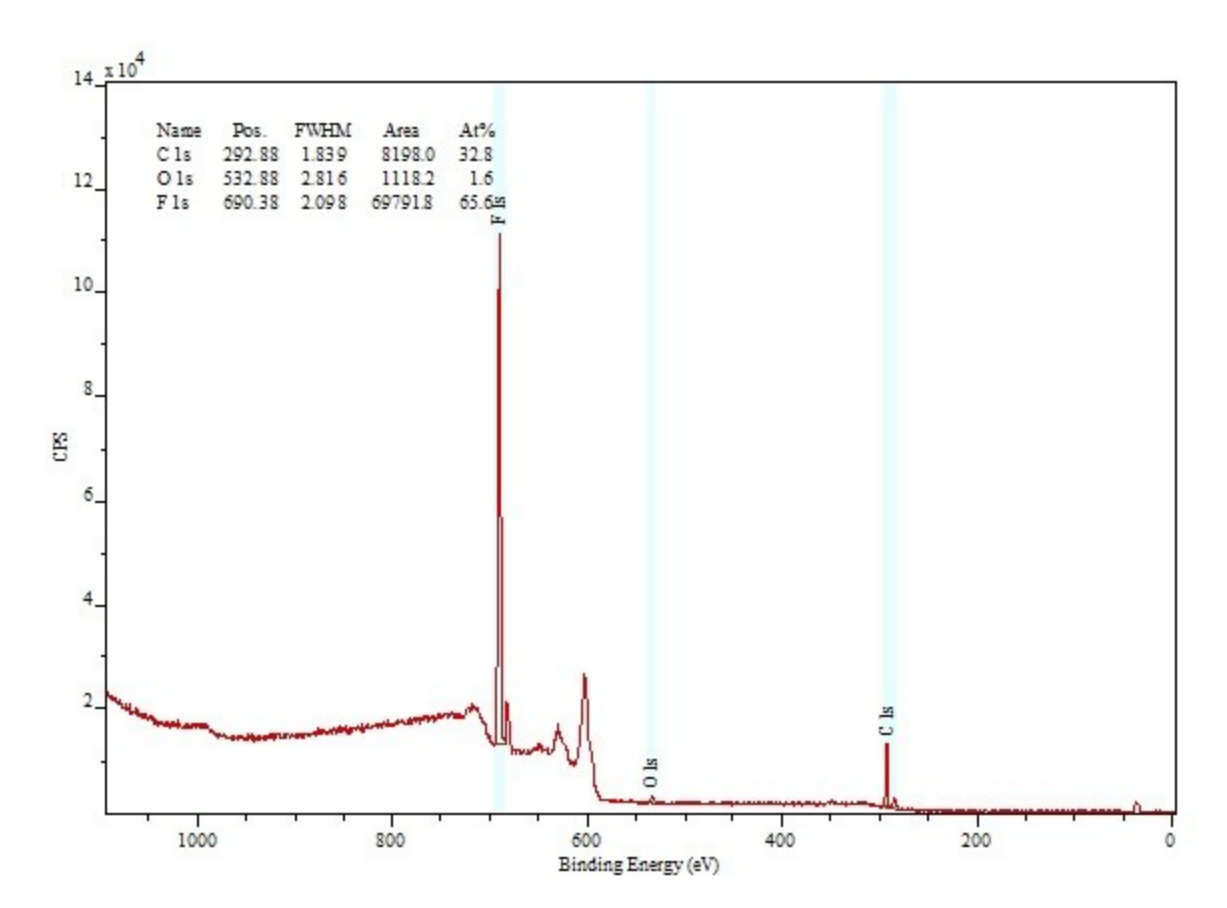


Figure 2

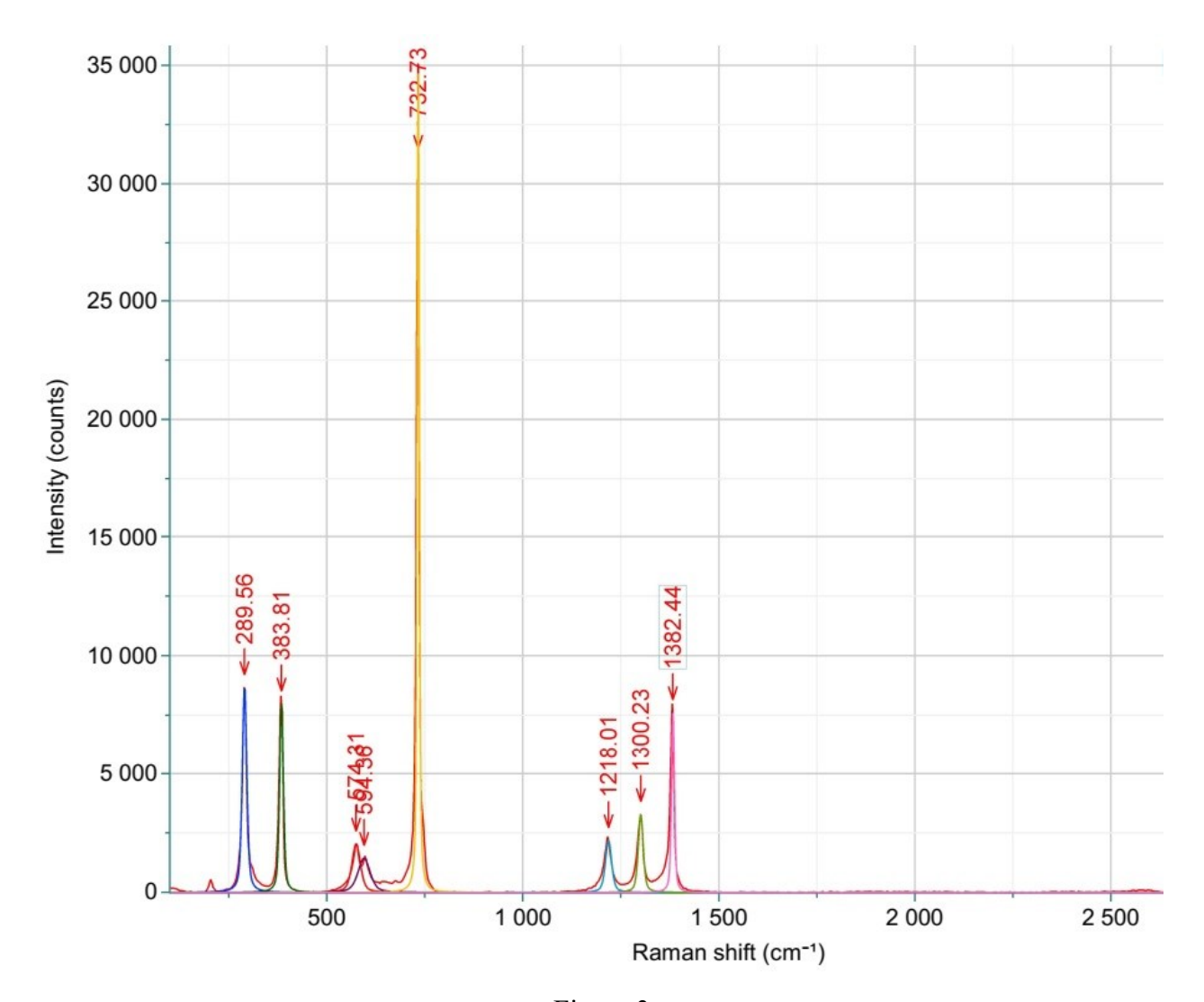
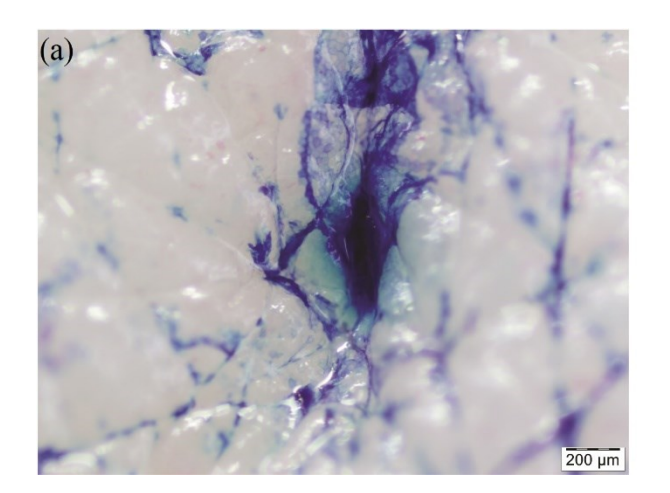


Figure 3



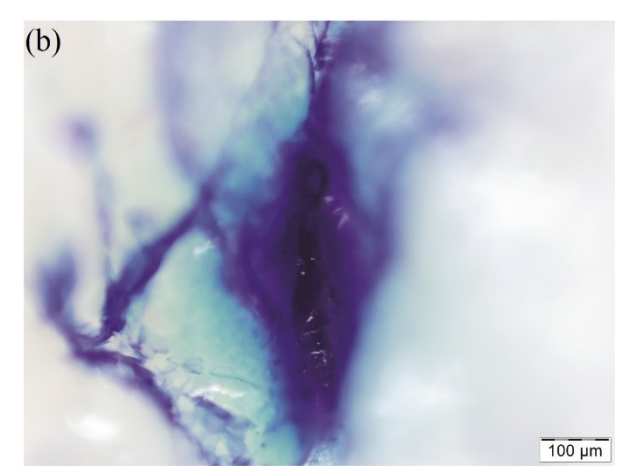


Figure 4